

pubs.acs.org/journal/ascecg Research Article

Highly Efficient Urea Oxidation via Nesting Nano-Nickel Oxide in **Eggshell Membrane-Derived Carbon**

Shun Lu, Matthew Hummel, Zhengrong Gu,* Yucheng Wang, Keliang Wang, Rajesh Pathak, Yue Zhou, Hongxing Jia, Xueqiang Qi,* Xianhui Zhao, Ben Bin Xu, and Xiaoteng Liu*



Cite This: https://dx.doi.org/10.1021/acssuschemeng.0c07614



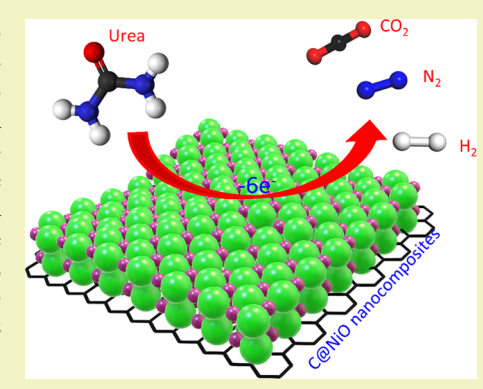
ACCESS

Metrics & More

Article Recommendations

Supporting Information

ABSTRACT: Here, we reported a strategy of using an eggshell membrane to produce hierarchically porous carbon as a low-cost substrate for synthesizing a nanonickel oxide catalyst (C@NiO), which can effectively turn biowaste—urea—into energy through an electrochemical approach. The interwoven carbon networks within NiO led to highly efficient urea oxidation due to the strong synergistic effect. The asprepared electrode only needed 1.36 V versus reversible hydrogen electrode to realize a high efficiency of 10 mA cm⁻² in 1.0 M KOH with 0.33 M urea and delivered an even higher current density of 25 mA cm⁻² at 1.46 V, which is smaller than that of the porous carbon and commercial Pt/C catalyst. Benefiting from theoretical calculations, Ni(III) active species and the porous carbon further enabled the electrocatalyst to effectively inhibit the "CO2 poisoning" of electrocatalysts, as well as ensuring its superior performance for urea oxidation.



KEYWORDS: nickel oxide, eggshell membrane, porous carbon substrate, urea oxidation, density functional theory

INTRODUCTION

In recent years, there has been a fast-growing trend in developing urea (CO(NH₂)₂) as a substitute H₂ carrier in energy conversion due to its high energy density, nontoxicity, stability, and nonflammability. Urea, a byproduct in the metabolism of proteins and a frequent contaminant in wastewater, is an abundant compound that has demonstrated favorable characteristics as a hydrogen-rich fuel source with 6.7 wt % gravimetric hydrogen content. 1-4 Also, there is 2-2.5 wt % urea from mammal urine; therefore, 0.5 million ton of additional fuels will be produced per year just from human urine (240 million ton each year). Electrochemical oxidation has been recognized as an efficient strategy for urea conversion and wastewater remediation. 9-11 Thus, the chemical energy harvested from urea/urine can be converted to electricity via urea oxidation reaction (UOR). 12-14 Moreover, the removal of urea from water is a priority for improving drinking water quality and presents an opportunity for UOR. 15 However, the transition of UOR from theory and laboratory experiments to real-world applications is largely limited by the conversion efficiency, catalyst cost, and feasibility of wide-spread usage.¹⁶

Primarily, electro-oxidation of urea has relied on costprohibitive rare metals such as ruthenium, platinum, tantalum, or iridium for urea catalysis. 14,17 Recent studies implementing common transition metals and their oxides, particularly nickel, have found similar success while having much lower material costs. 18-20 For instance, Luo et al. prepared ultrathin and

porous nickel hydroxide nanosheets for efficient UOR and found that 1.82 V (vs reversible hydrogen electrode (RHE)) was needed to achieve a large current density of 298 mA cm⁻².²¹ Qiao et al. reported a two-dimensional nickel-based metal-organic framework (2D Ni-MOF) nanosheets by coordinating nickel ions and benzenedicarboxylic acid. The electrochemical results showed better UOR performance and smaller overpotential compared to Ni(OH)₂ and commercial Pt/C.¹³ Similarly, Ma et al. investigated Ni-MOF with different morphologies, such as nanowires, neurons, and urchins, and found that the Ni-MOF nanowires require ~0.8 V (vs Ag/AgCl) to obtain a current density of 160 mA cm⁻².²² Thus, based on the previous studies, the nickel-based materials' electrocatalytic behavior is well understood, making them ideal candidates for UOR. 23,24 However, there is still sluggish kinetics of UOR at the anodic area owing to the multielectron transfer and multiple gas adsorption/desorption procedures. 23-27 To address this key issue, the coordination of high surface area and conductive materials are considered beneficial for expanding the electrochemically active surface area.²⁸⁻³⁰ The bioderived carbon-doped nickel can provide

Received: October 16, 2020 Revised: December 22, 2020





Figure 1. Scheme of the formulation process of the porous C@NiO nanocomposites: (a) dried NiO/ESM after the hydrothermal process, (b) pyrolysis treatment, and (c) final product after the pyrolysis.

the electrochemically active high surface area and conductivity in the material selection, resulting in efficient substrates.³¹ Innovations with UOR from organic and bioderived compounds have yielded substantial improvements in energy production efficiency.^{32,33}

Biomass-derived carbon materials have been increasingly implemented in electrochemical energy conversion and detection owing to their low price, porous structure, and high conductivity.³⁴ Hierarchical porous activated carbons are favored, in particular, due to variations in their pore size and volume, the potential for modification, and synthesis from waste biomaterials. 35,36 One promising material that has demonstrated notable electrochemical properties is the eggshell membrane (ESM). ESM is a thin, protein-based membrane functioning as a gas-exchange interface for the embryo within the egg to the outside world via its abundant micro- and nanosized pores.³⁷ Aside from the traditional methods of waste management, ESM has been used in the production of clean energy where it replaces coal, oil, or natural gases to generate electricity through fuel cell devices. ESM collected from waste eggshells has demonstrated excellent electrochemical behavior on its own in energy storage and conversion^{38,39} as well as an ability to be infused with different transition-metal oxides for sensing purposes. 40,41

In this work, we reported a low-cost UOR electrocatalyst (C@NiO) composed of nickel oxide nanoparticles anchored on the porous carbon derived from the biowaste eggshell membrane via hydrothermal synthesis and pyrolysis. Benefiting from the strong synergistic effect between nickel oxide and porous carbon, the as-prepared electrode only needs 1.36 V versus RHE to realize 10 mA cm⁻² in a 1.0 M alkali solution containing 0.33 M urea and delivers 25 mA cm⁻² at 1.46 V. In addition, in the viewpoint of the theoretical calculations, its intermediate (C@NiOOH), which is formed from C@NiO in an alkaline solution, made this electrocatalyst to possess the

ability to effectively hinder " CO_2 poisoning", as well as ensuring its superior performance for UOR. This work also presented a low-cost urea oxidation electrocatalyst design with a porous structure to solve the problems we described previously (source and cost) and promote the catalyst's potential application in energy conversion based on the concept of "trash to treasure".

EXPERIMENTAL SECTION

Preparation of the Porous C@NiO Nanocomposites. Before obtaining C@NiO nanocomposites from the biowaste eggshell membrane, the ESM received pretreatment to remove the left egg white and other organic chemicals. C@NiO nanocomposites were prepared through a smart approach that not only the eggshell was employed as a reactor but also the eggshell membrane as a filter membrane here, as presented in Figure 1. First, the eggshell filled with Ni(NO₃)₂ aqueous solution was transferred into a beaker with urea and then kept at 70 °C for 6 h. In this process, Ni(OH)2 was synthesized at the interface of the eggshell membrane as OH⁻ ions (outside of ESM) were reacted with Ni²⁺ ions (inside of ESM). Then, the eggshell membrane was stripped from the eggshell reactor by tweezers after the reaction system was naturally cooled down. The stripped ESM was washed thoroughly with deionized water. Completely, black powder was received after calcination at 500 °C for 2 h in a N_2 environment. The calcined black powder with a metallic color was washed and collected for further characterizations.

Physical Characterizations. Scanning electron microscopy (SEM) and transmission electron microscopy (TEM) were both employed to observe the morphological information of the asprepared samples, equipped with high-resolution TEM (HRTEM) and selected area electron diffraction (SAED). Scanning transmission electron microscopy—energy dispersive X-ray (STEM—EDX) spectroscopy was employed for analyzing the distribution of elements. The pyrolysis process was investigated to indicate the synthesis of C@NiO nanocomposites through the thermogravimetric analysis (TGA) measurement in a nitrogen gas environment. TGA was performed by an integrated thermal analyzer with a ramp rate of 20 $^{\circ}$ C min $^{-1}$ under N_2 protection. Furthermore, X-ray diffraction

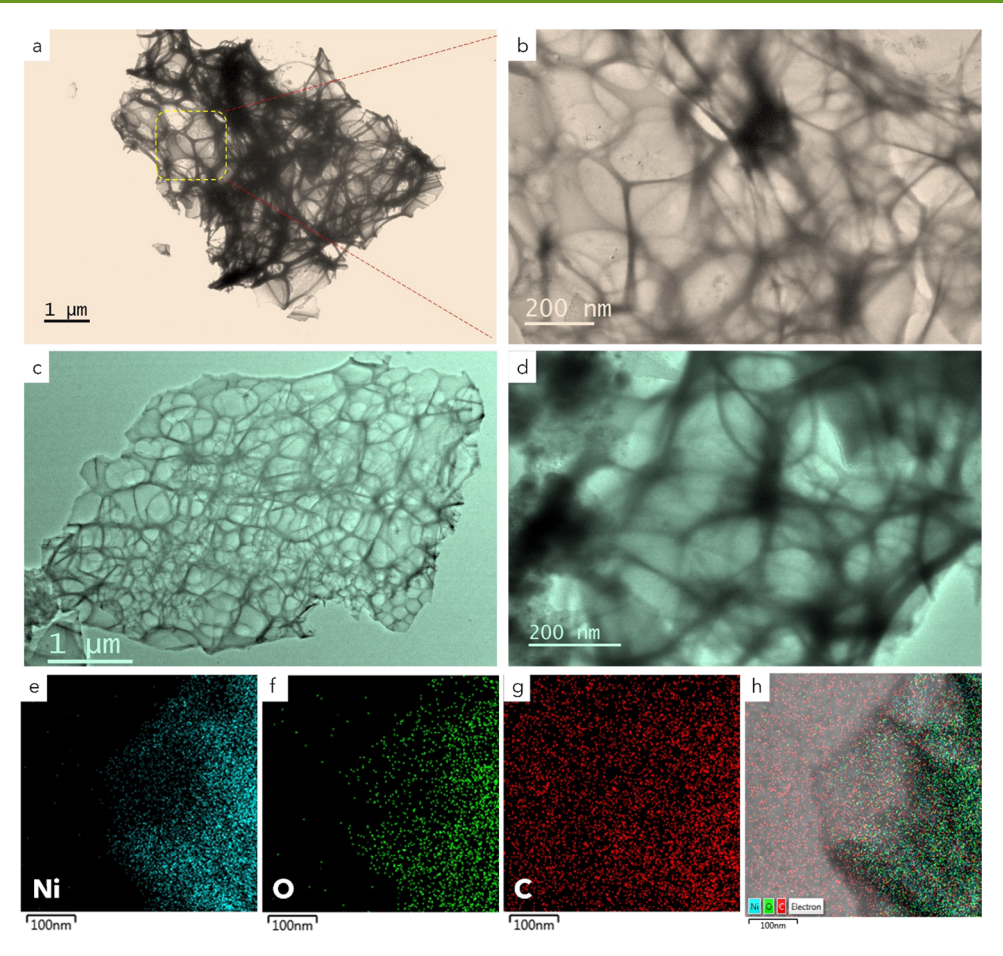


Figure 2. (a, b) TEM images of the porous carbon. (c, d) TEM images and (e-h) STEM-EDX images of the C@NiO nanocomposites.

(XRD) was used for analyzing the crystalline structure of the asobtained sample. X-ray photoelectron spectroscopy (XPS) spectra were recorded to analyze the surface composition and chemical valence information of the as-prepared sample. All binding energies were referred to as the C 1s peak of surface adventitious carbon at 284.8 eV.

Electrochemical Measurements. All electrochemical measurements of urea oxidation were performed on a CHI (760E, Texas) electrochemical analyzer. The conventional three-electrode testing configuration was used in all electrochemical measurements. A glassy carbon electrode (Ø 3 mm) was used as the working electrode (WE) and would receive catalyst modification, A Pt electrode and Ag/AgCl (within saturated KCl solution) were selected as the counter and reference electrode (CE and RE), respectively. Considering different concentrations of urea used for oxidation, such as 0.1, 0.33, and 0.5 M, 0.33 M urea was selected for oxidation measurements in this study to match the concentration in mammal urine. 42,43 Cyclic voltammetry (CV) and linear sweep voltammetry (LSV) or polarization measurements were both carried out in a 1.0 M alkali solution with/without 0.33 M urea. The electrochemical impedance spectroscopy (EIS) spectrum was also investigated in a 0.1 M potassium ferricyanide solution (frequency range, 100 kHz to 0.1 Hz; AC perturbation, 5 mV; applied potential, open-circuit potential). Electrochemical double-layer capacitance (C_{dl}) tests were performed through a series of CV tests using a series of scan rates (2-10 mV s^{-1}) in 1.0 KOH with a similar potential range (0.06–0.16 V vs Ag/ AgCl). Chronoamperometry (CA) measurements were carried out at a constant potential vs Ag/AgCl for 1800 s in 1.0 alkali media with 0.33 M urea. Here, the loading mass of the catalyst on the working electrode was calculated as 0.075 mg cm⁻², and all potentials mentioned in this study were converted *versus* a reversible hydrogen electrode (RHE): $(E_{\rm RHE} = E_{\rm Ag/AgCl} + 0.21 \text{ V} + 0.059 \times \text{pH}, 25^{\circ}\text{C})$

unless otherwise specified, and iR compensation was performed for all linear LSV results.

Density Functional Theory (DFT) Calculation Methods. To study the source of the highly electrocatalytic performance of C@ NiO nanocomposites, calculations were carried out using spinpolarized density functional theory (DFT), equipped with the CASTEP package with the Perdew-Burke-Ernzerh (PBE) formulation of the generalized gradient approximation (GGA).44 The adsorption of urea and CO2 on C@NiO was studied compared with that on C@NiOOH, and the heterojunctions were chosen as our theoretical models. The core electrons were treated with ultrasoft pseudopotentials.⁴⁵ The cutoff energy for the plane wave expansion was 340 eV, and the Monkhorst-Pack k-point sampling was generated with a $2 \times 2 \times 1$ grid. The convergence criterion for the structural optimizations was a maximum force of 0.05 eV/Å and a maximum displacement of 0.002 Å. A vacuum layer of 15 Å thickness was used along the z-direction to totally eliminate the interactions between different surfaces. The adsorption energy of urea or CO2 over C@NiO and C@NiOOH was calculated according to eq 1

$$E_{\rm ads} = E_{\rm total} - (E_{\rm slab} + E_{\rm adsorbate}) \tag{1}$$

where $E_{\rm ads}$ is the adsorption energy, $E_{\rm total}$ is the total energy for the adsorption state, $E_{\rm slab}$ is the energy of the optimized surface of C@ NiO or C@NiOOH, and $E_{\rm adsorbate}$ is the energy of a single urea or CO₂ molecule.

■ RESULTS AND DISCUSSION

Physical Characterizations of the Porous C@NiO Nanocomposites. There is a hierarchical structure of the porous carbon with transparent layers between carbon frameworks (Figure 2a,b), indicating that it can provide a

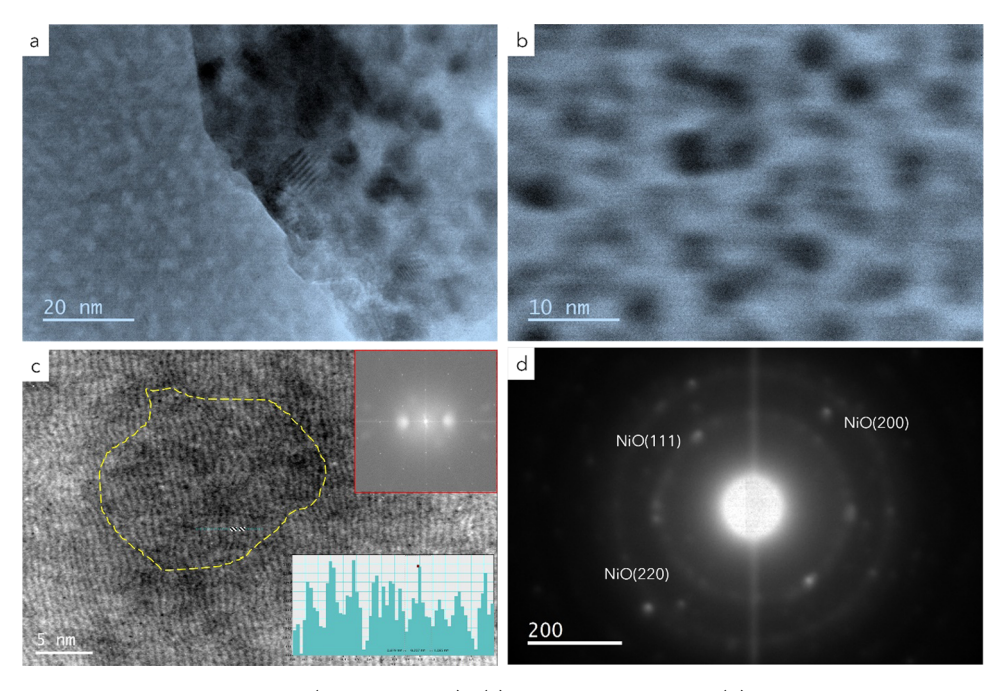


Figure 3. (a, b) TEM images with magnifications (20 and 10 nm), (c) HRTEM image, and (d) SAED pattern of C@NiO nanocomposites.

large surface area for active sites. 46 As depicted in Figure 2c, NiO nanoparticles are anchored on the porous carbon frameworks. The color of carbon layers tends to dark (Figure 2d), which differs from that in Figure 2b. This phenomenon may be due to the introduction of NiO nanoparticles. STEM-EDX mapping was further applied to verify the composition of the as-prepared sample. The element distribution of Ni, O, and C without other impurities on the transparent layers is observed well with higher magnification (~100 nm) in Figure 2e-h. That porous structure is derived from the biomacromolecule fibers of ESM, 38 with NiO nanoparticles dispersed well on the porous carbon, as presented in Figure 2g.

Several black dots with an average size of 6.5 nm are displayed in Figure 3a,b, confirming the existence of NiO nanoparticles. Figure 3c exhibits an average lattice spacing of 0.207 nm in the dark area, which corresponds to the (111) facet of NiO (JCPDS no. 47-1049). Figure S1 also presents several similar areas with the same lattice spacing from Figure 3c. Meanwhile, NiO grains encapsulated on porous carbon also can be confirmed by its lattice fringes using fast Fourier transform (FFT) of HRTEM images due to NiO having specified unit cell parameters of 0.418 nm with face-centered cubic (fcc) structures (inset of Figure 3c). As a comparison, pure NiO particles were synthesized using the same method and their morphology showed aggregates of different sizes (Figure S2) due to no support in hydrothermal treatment for good dispersion.⁴⁷ The SAED result of C@NiO nanocomposites in Figure 3d reveals the polycrystalline property with the feature of uniform central and diffraction spots. The diffraction rings correspond to the diffraction of the graphitelike carbon, and the appeared spots are indexed to (111), (200), and (220) diffraction of pure NiO. All of the above results demonstrated that the porous C@NiO nanocomposite was successfully prepared with a hierarchical structure and uniform dispersion.

The TGA result of the precursor $Ni(OH)_2/ESM$ is presented in Figure S3. The precursor $Ni(OH)_2/ESM$

endured a four-step weight loss owing to continuous dehydration and decomposition. The first stage (20-100 °C) is related to the evaporation of adsorbed and intercalated water molecules associated with the surface of Ni(OH)₂/ ESM. It is possible to estimate the water content (10 wt %) of the precursor. ESM started pyrolyzing at ~200 °C and was completely pyrolyzed at 550 °C with a weight loss of 48 wt %. Similarly, Zhai et al. found that the decomposition of Ni(OH)₂ into NiO occurs between 300 and 400 °C. 48 For this step, the TG curve exhibits a sharp weight loss with 19 wt %, which is in line with the theoretical weight loss value (19.4%) due to the decomposition of Ni(OH)2.49 Organic components are completely removed in this stage, including gas like CO2, resulting in the uniformed NiO nanoparticles anchoring on porous carbon. This result is well consistent with previous TEM and SEM observations.

In Figure 4a, the peaks appearing at 37.2, 43.2, and 62.8° (2θ) are indexed to the crystal planes of NiO (JCPDS card #47-1049) well. The peaks at 24.8° also confirmed the existence of carbon (JCPDS card #41-1487). This XRD analysis identified the presence of NiO and C in the asprepared sample, which also remains consistent with the HRTEM pattern. The XPS survey spectrum of C@NiO nanocomposites further confirms the existence of nickel, oxygen, and carbon species in Figure 4b. There are two apparent peaks located at 873.3 and 855.8 eV due to Ni 2p_{1/2} and Ni 2p_{3/2}, as depicted in Figure 4c. As a result, the binding energy peaks at 880 eV and 861 eV are assigned to the satellite peaks of Ni 2p_{1/2} and Ni 2p_{3/2}, respectively. The spinenergy separation of two main peaks (from 873.3 to 855.8 eV) is \sim 17.5 eV, which is the typical characteristic of the Ni(OH)₂ phase, 48 Nevertheless, all of the Ni 2p peaks of the asprepared sample shift to higher binding energies compared to Ni(OH)2, implying a higher oxidation state of Ni(II) ions in C@NiO nanocomposites.¹³ C 1s can be further fitted to three peaks located at 286.4, 285.8, and 284.2 eV, corresponding to the carbonyl bond, carbon-oxygen bond, and carbon-carbon bond in Figure 4d. The above results further confirmed the

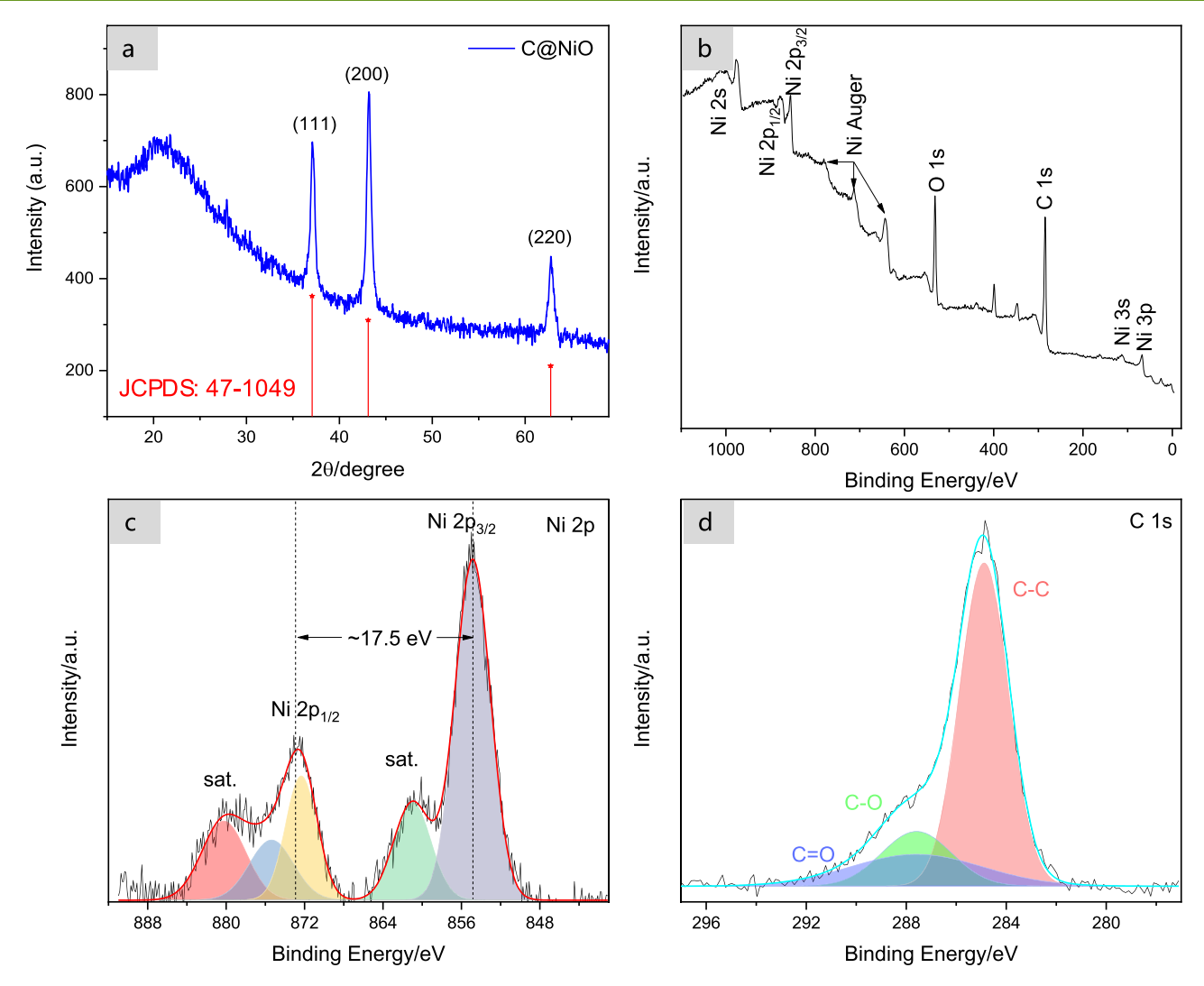


Figure 4. (a) XRD pattern, (b) XPS survey spectrum, and the high-resolution XPS spectra of (c) Ni 2p and (d) C 1s regions of C@NiO nanocomposites.

successful growth of NiO nanoparticles anchored on the porous carbon to prepare C@NiO nanocomposites.

UOR Performance of the Porous C@NiO Nano-composites. To assess the electrocatalytic performance of C@NiO nanocomposites for urea oxidation, electrochemical measurements were applied through a typical three-electrode setting. A urea electrolysis reaction in an alkaline environment can be expressed as follows (eqs 2–4)

Anode:

$$CO(NH_2)_2 + 6OH^- \rightarrow N_2 + 5H_2O + CO_2 + 6e^-$$
(2)

Cathode:

$$2H_2O + 2e^- \rightarrow H_2 + 2OH^-$$
 (3)

Overall:

$$CO(NH_2)_2 + H_2O \rightarrow N_2 + 3H_2 + CO_2$$
 (4)

The electrochemical behaviours of the C@NiO electrode were evaluated by CV measurements in the alkaline medium in the absence/presence of 0.33 M urea, and those of the pure NiO sample and the porous carbon electrode were also tested for comparison, as shown in Figure S4. As for the C@NiO

electrode, there is an obvious oxidation peak at \sim 1.32 V, which can be attributed to the formation of NiOOH species.²⁵ However, the C@NiO electrode presents an improved current density for urea oxidation after the addition of urea. Coincidentally, the onset potential of UOR is very close to the potential position, where NiOOH species are generated, implying that the fresh NiOOH species acted as active sites for urea oxidation, which is consistent with the reported Ni-based electrocatalysts. ^{13,41,47,50} Furthermore, the integrated area of CV of the C@NiO electrode is larger than that of the porous carbon electrode, indicating that NiO nanoparticles anchoring the porous carbon exposed more active species for urea oxidation and enhanced the electrocatalytic performance of UOR. Figure 5a reveals the linear sweep voltammetry curves of the C@NiO electrode compared with those of the porous carbon and commercial 20% Pt/C in the alkali media containing 0.33 M urea. The current density of the C@NiO electrode increases with the potential to move toward the positive side, while the other two samples only show minor changes. The UOR catalytic performance of C@NiO is estimated by Tafel curves in Figure 5b. A more intuitional comparison of potential (the current density of 10 mA cm⁻²) and Tafel information among the C@NiO electrode, porous carbon, and commercial 20% Pt/C could be found in the

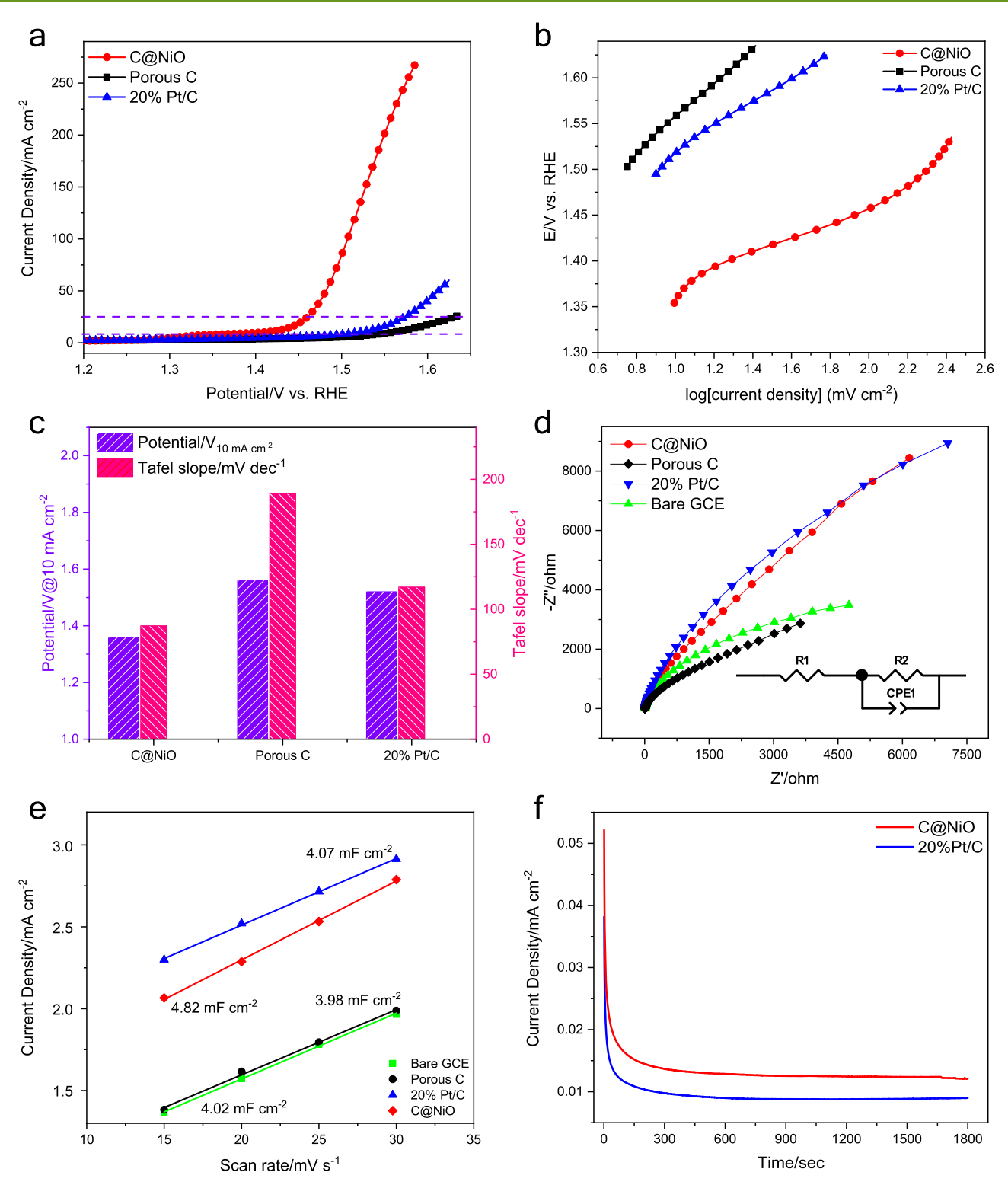


Figure 5. Electrochemical performance for UOR. (a) LSV curves of porous carbon, 20% Pt/C, and C@NiO electrodes in 1.0 M KOH containing 0.33 M urea; (b) Tafel plots of the above samples; (c) histogram of the comparison of the potentials and Tafel slopes between the porous carbon, 20% Pt/C, and C@NiO electrodes; (d) Nyquist plots of porous carbon, 20% Pt/C, and C@NiO electrodes in 1.0 M KOH with an open-circuit voltage; (e) linear plots of double-layer capacitance to assess the electrochemically active surface area; (f) chronoamperometry curves of C@NiO and 20% Pt/C in 1.0 M KOH containing 0.33 M urea at an applied potential of 1.3 V (vs RHE).

histogram (Figure 5c), in which the C@NiO electrode presents the lowest potential to attain 10 mA cm⁻². The Tafel slope of C@NiO (87.2 mV dec⁻¹) is also lower than those of the porous carbon and commercial Pt/C, implying faster UOR kinetics for the C@NiO electrode. As presented

in Table S1, the UOR performance of several electrocatalysts was listed. The C@NiO electrode presents a smaller potential and lower mass loading than those of the porous carbon and commercial Pt/C, suggesting its favorable reaction kinetics for UOR.

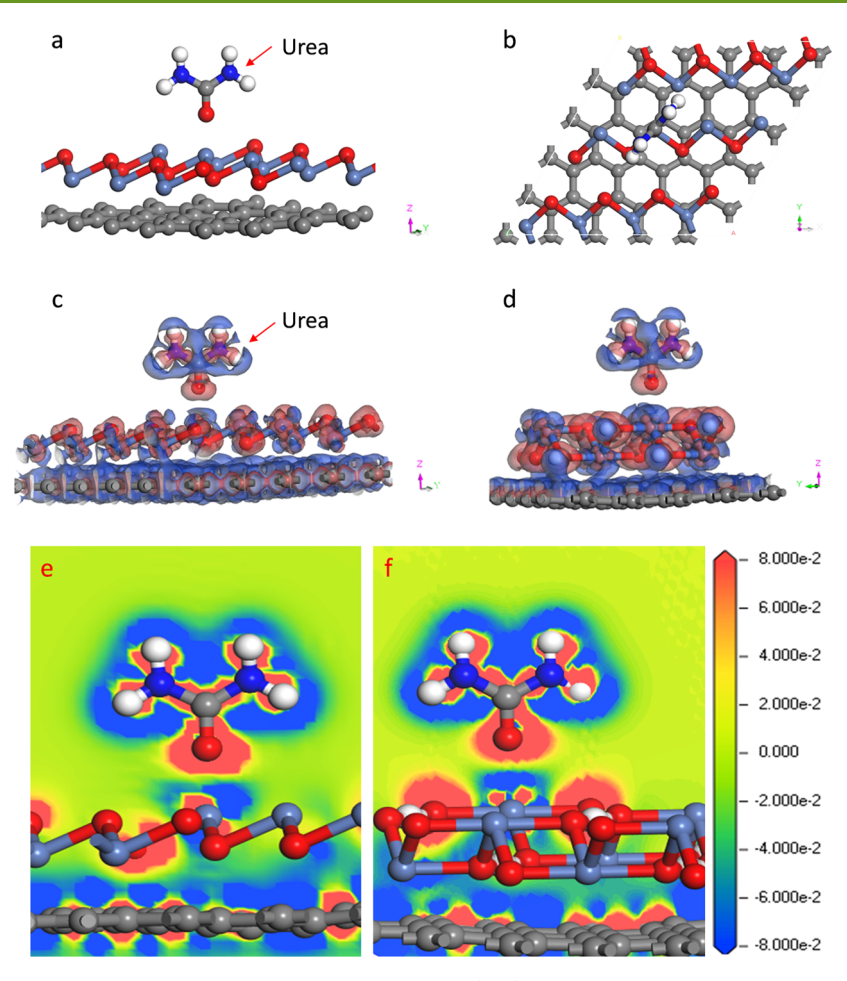


Figure 6. Structural model of porous C@NiO and urea under different views (a, b). Electron density difference of urea adsorbed on (c) C@NiO and (d) C@NiOOH; the red hooded face means the enrichment of electrons, while the blue one means the deficiency of electrons. Slice images of the adsorption of urea molecule on the surface of (e) C@NiO and (f) C@NiOOH heterojunctions and the corresponding slice of the electron density difference. The contour around the atoms represents electron accumulation (red) or electron deletion (blue).

Mechanism Investigation via Electrochemical Measurements. EIS measurements were also tested to obtain more information about the catalytic performance of C@NiO nanocomposites. Porous carbon, 20% Pt/C, and the bare glassy carbon electrode (GCE) all received the same test as a comparison. The results presented in Figure 5d indicate that the C@NiO electrode presents a much smaller Nyquist semicircle than that of porous carbon, 20% Pt/C, and bare GCE under an open-circuit potential, revealing that it has a much faster charge transfer than the other samples, which well matches with the previous polarization curves. Electrochemical active surface area (ECSA) measurements were further performed to study the electrochemical double-layer capacitance $(C_{\rm dl})$ among C@NiO, porous carbon, 20% Pt/C, and the bare GCE. As demonstrated in Figure 5e, the C@NiO electrode was calculated to be 4.82 mF cm⁻², well above the values of porous carbon (3.98 mF cm⁻²), 20% Pt/C (4.07 mF cm⁻²), and the bare GCE (4.02 mF cm⁻²). Calculation details can be found in Figure S5. This means that the C@NiO electrode has a larger active surface area with more active sites that promote UOR efficiently. In addition, the presence of urea increases the current density of the anode as the potential is also applied. As presented in Figure S6, the current density of the C@NiO electrode presents the stepwise increasing potential in the 1.0 M alkali solution with/without 0.33 M urea. When the positive potential (0.1-0.4 V vs Ag/AgCl) is

applied, there are no redox cycles corresponding to the conversion of $\mathrm{Ni^{2+}}$ species to $\mathrm{Ni^{3+}}$ species before urea addition. When a potential (0.5–0.8 V νs Ag/AgCl) larger than the onset potential was applied, a higher current density can be obtained owing to the oxygen enhancement ratio (OER) effect. It can be inferred that the porous C@NiO nanocomposites induce high electron transfer and mass transport due to their excellent electrical conductivity.

Moreover, the stable multistep chronopotentiometry (CP) curves also suggest better conductivity and mass transport of the C@NiO electrode for UOR performance. The stability of the C@NiO electrode during urea oxidation was further examined, as shown in Figure 5f. It can be observed that the current density of the C@NiO electrode only shows negligible degradation compared with commercial 20% Pt/C after 1800 s testing under an applied potential of 1.3 V vs RHE. This indicates that the C@NiO electrode has good catalytic stability in alkali with urea. To further confirm the structural stability after long-term durability, the stripped sample from the working electrode was observed again by the TEM technique. It keeps the original layer structure with uniform NiO nanoparticles, as demonstrated in Figure S7. Consequently, it can be concluded that the C@NiO electrode shows excellent UOR performance because (i) NiO nanoparticles directly anchored on porous carbon could enlarge the electrochemically active surface area and (ii) the transparent

carbon layer could enhance its electrical conductivity, providing faster electron transfer and mass transport between nanoparticles and the carbon matrix, improving UOR electrocatalytic performance, reducing NiO nanoparticle contact with electrolyte directly, and thereby enhancing the stability.

Mechanism Investigation via Theoretical Calculations. To gain insight into the synergistic effect in C@NiO nanocomposites towards urea oxidation, spin-polarized DFT calculations were utilized to provide more details in this work. Generally, CO(NH₂)₂ is primarily adsorbed on the surface of electrocatalysts during urea electro-oxidation. It indicates that the adsorption energy of urea plays an important function in determining the electrocatalytic urea oxidation.⁵¹ It is noteworthy that our DFT calculations do not take all the experimental details into account, and the graphene was present as an alternative structure to simulate the porous carbon, qualitatively revealing the influence of the porous structure on the electronic structure of NiO nanoparticles. The graphene/NiOOH and graphene/NiO heterojunctions were chosen as the theoretical models in this work (Figure 6a,b). According to the DFT calculations, the urea preferred to adsorb on the surface of C@NiOOH heterojunction and the adsorption energy is -1.53 eV, while the adsorption energy is only -0.97 eV on the C@NiO heterojunction (Figure S8a). Moreover, the electron density difference shown in Figure 6c,d and the slight electron density difference in Figure 6e,f showed that a little bit more electrons from Ni transfer to the O atom of urea on the C@NiOOH heterojunction than that on the C@NiO heterojunction, which means that the alkaline environment plays an important role in the UOR. Also, it can be deemed that the Ni(III) species presented its favorable active sites.

Besides, CO₂ adsorption on the surface or at the interface of catalysts is significant to the remarkable UOR performance.⁵² Moreover, the rate-determining step in UOR is the adsorbed CO₂ desorption from active sites.⁵³ Thus, the adsorption energy of CO2 on the C@NiO electrode and C@ NiOOH was comparatively studied with DFT calculations. As illustrated in Figure S8b, it can be determined that the adsorption energy of CO2 on C@NiO is -0.57 eV, while it becomes almost zero on the C@NiOOH surface, which means much weaker CO2 adsorption over C@NiOOH. Furthermore, the calculated d band center of Ni in C@NiO is -1.97 eV, while it goes far from the Fermi level and decreases to -2.20 eV for Ni in C@NiOOH (Figure S8c). The lower d band center leads to weaker adsorption for CO₂. From this viewpoint, it enables to effectively retard the CO₂ poisoning of the electrocatalyst, ensuring its superior UOR performance.

UOR Performance Enhancement Mechanism Discussion. The improvement of UOR performance is mainly benefitted from the synergistic effect between NiO and porous carbon, as illustrated in Figure 7. It can be ascribed to several reasons, as follows: (i) NiO nanoparticles directly encapsulated onto the porous carbon enlarged the electrochemically active surface area with more active sites. For example, three-dimensional (3D) interwoven-like structures could afford more active sites and enable gas release for reactions in the viewpoint of material preparation. (ii) The transparent carbon layer could enhance its electrical conductivity, providing faster electron transfer and mass transport between nanoparticles and the carbon matrix, improving UOR electrocatalytic

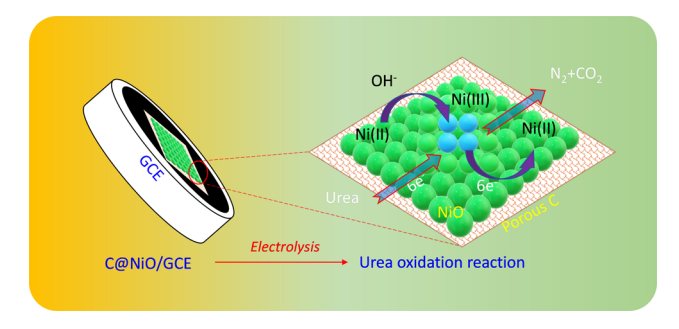


Figure 7. Mechanism of UOR on the C@NiO electrode.

performance, reducing NiO nanoparticles contact with electrolyte directly, therefore enhancing the stability. (iii) The synergistic effect in C@NiO nanocomposites could regulate the electron density to optimize active sites and promote electrocatalytic UOR performance efficiently in terms of theoretical calculations.

CONCLUSIONS

In summary, we have reported the nickel oxide nanoparticles supported on the carbonized eggshell membrane with interwoven networks as low-cost electrocatalysts (C@NiO) toward urea oxidation. The resulting C@NiO electrode exhibited much better electrocatalytic urea oxidation performance than that of commercial 20% Pt/C under the same test conditions. It can achieve a current density of 10 mA cm⁻² at 1.36 V (vs RHE) and 25 mA cm⁻² at 1.46 V (vs RHE) and a low Tafel slope of 87.2 mV dec⁻¹. Such an excellent urea oxidation performance could be attributed to the synergetic effect in the porous carbon and NiO nanoparticles that provides excellent electrocatalytic activity and stability in the C@NiO nanocomposites. Moreover, benefitting from theoretical calculations, Ni(III) species and porous carbon further enabled the electrocatalyst to effectively inhibit the CO2 poisoning of electrocatalysts, guaranteeing its superior UOR performance. This study may promote a low-cost UOR electrocatalyst design with a porous structure and uniform composition and develop biomass-derived applications in urea conversion based on the concept of trash to treasure.

ASSOCIATED CONTENT

Supporting Information

The Supporting Information is available free of charge at https://pubs.acs.org/doi/10.1021/acssuschemeng.0c07614.

HRTEM image of C@NiO nanocomposites; SEM images of NiO particles and the porous carbon; TGA curve of C@NiO nanocomposites; comparison of CV results for NiO, porous carbon, and C@NiO nanocomposites in the absence and presence of urea in the alkaline solution; CV curves of the GCE, porous carbon, Pt/C and C@NiO nanocomposites in a narrow range; current response at different potentials on the C@NiO electrode; TEM images of C@NiO nanocomposites after urea oxidation; adsorption energy of urea/CO2 on porous C@NiO and C@NiOOH; d density of states of Ni in NiO and NiOOH; and comparison of the UOR performance and mass loadings between recently reported electrocatalysts (PDF)

AUTHOR INFORMATION

Corresponding Authors

Zhengrong Gu − Department of Agricultural and Biosystems Engineering, South Dakota State University, Brookings, South Dakota 57007, United States; orcid.org/0000-0003-1860-2651; Email: zhengrong.gu@sdstate.edu

Xueqiang Qi — College of Chemistry and Chemical Engineering, Chongqing University of Technology, Chongqing 400054, China; Email: xqqi@cqut.edu.cn

Xiaoteng Liu — Department of Mechanical & Construction Engineering, Faculty of Engineering and Environment, Northumbria University, Newcastle upon Tyne NE1 8ST, U.K.; ⊙ orcid.org/0000-0001-7574-1709; Email: Terence.liu@northumbria.ac.uk

Authors

Shun Lu – Department of Agricultural and Biosystems Engineering, South Dakota State University, Brookings, South Dakota 57007, United States; Department of Mechanical & Construction Engineering, Faculty of Engineering and Environment, Northumbria University, Newcastle upon Tyne NE1 8ST, U.K.

Matthew Hummel — Department of Agricultural and Biosystems Engineering, South Dakota State University, Brookings, South Dakota 57007, United States;
ocid.org/0000-0002-9576-1309

Yucheng Wang — Department of Mechanical & Construction Engineering, Faculty of Engineering and Environment, Northumbria University, Newcastle upon Tyne NE1 8ST, U.K.

Keliang Wang — Department of Electrical Engineering and Computer Engineering & Department of Chemical Engineering and Materials Science, Michigan State University, East Lansing, Michigan 48824, United States; orcid.org/0000-0002-3273-9075

Rajesh Pathak — Department of Electrical Engineering and Computer Science, South Dakota State University, Brookings, South Dakota 57007, United States

Yue Zhou – Department of Electrical Engineering and Computer Science, South Dakota State University, Brookings, South Dakota 57007, United States

Hongxing Jia — Department of Agricultural and Biosystems Engineering, South Dakota State University, Brookings, South Dakota 57007, United States

Xianhui Zhao — Manufacturing Science Division, Oak Ridge National Laboratory, Oak Ridge, Tennessee 37831, United States; © orcid.org/0000-0002-0282-5810

Ben Bin Xu — Department of Mechanical & Construction Engineering, Faculty of Engineering and Environment, Northumbria University, Newcastle upon Tyne NE1 8ST, U.K.; © orcid.org/0000-0002-6747-2016

Complete contact information is available at: https://pubs.acs.org/10.1021/acssuschemeng.0c07614

Notes

The authors declare no competing financial interest.

ACKNOWLEDGMENTS

This work is supported by NASA EPSCoR (no. NNX16A-Q98A), NSF/EPSCoR (no. OIA-1849206), the U.K. Engineering Physics and Science Research Council (Grant No. EP/S032886/1), the Foundation and Frontier Research

Project of Chongqing of China (cstc2018jcyjAX0513), and the Science and Technology Research Program of Chongqing Municipal Education Commission (KJQN201801125). In addition, S.L. thanks to Yuehui Wang's care during Shun's Ph.D. period. This manuscript has been authored in part by UT-Battelle, LLC, under contract DE-AC05-00OR22725 of the U.S. Department of Energy (DOE). The US Government retains—and the publisher, by accepting the article for publication, acknowledges that the US government retains—a nonexclusive, paid-up, irrevocable, worldwide license to publish or reproduce the published form of this manuscript or allow others to do so for US government purposes. DOE will provide public access to these results of federally sponsored research in accordance with the DOE Public Access Plan (http://energy.gov/downloads/doe-public-access-plan).

REFERENCES

- (1) Zhang, J.-Y.; He, T.; Wang, M.; Qi, R.; Yan, Y.; Dong, Z.; Liu, H.; Wang, H.; Xia, B. Y. Energy-saving hydrogen production coupling urea oxidation over a bifunctional nickel-molybdenum nanotube array. *Nano Energy* **2019**, *60*, 894–902.
- (2) Rollinson, A. N.; Jones, J.; Dupont, V.; Twigg, M. V. Urea as a hydrogen carrier: a perspective on its potential for safe, sustainable and long-term energy supply. *Energy Environ. Sci.* **2011**, *4*, 1216–1224
- (3) Chen, S.; Duan, J.; Vasileff, A.; Qiao, S. Z. Size Fractionation of Two-Dimensional Sub-Nanometer Thin Manganese Dioxide Crystals towards Superior Urea Electrocatalytic Conversion. *Angew. Chem., Int. Ed.* **2016**, 55, 3804–3808.
- (4) Sha, L.; Ye, K.; Wang, G.; Shao, J.; Zhu, K.; Cheng, K.; Yan, J.; Wang, G.; Cao, D. Hierarchical $NiCo_2O_4$ nanowire array supported on Ni foam for efficient urea electrooxidation in alkaline medium. *J. Power Sources* **2019**, *412*, 265–271.
- (5) Yue, Z. H.; Yao, S. Y.; Li, Y. Z.; Zhu, W. X.; Zhang, W. T.; Wang, R.; Wang, J.; Huang, L. J.; Zhao, D. Y.; Wang, J. L. Surface engineering of hierarchical Ni(OH)₂ nanosheet@nanowire configuration toward superior urea electrolysis. *Electrochim. Acta* **2018**, 268, 211–217.
- (6) Urbańczyk, E.; Maciej, A.; Stolarczyk, A.; Basiaga, M.; Simka, W. The electrocatalytic oxidation of urea on nickel-graphene and nickel-graphene oxide composite electrodes. *Electrochim. Acta* **2019**, 305. 256–263.
- (7) Radenahmad, N.; Afif, A.; Petra, P. I.; Rahman, S. M.; Eriksson, S.-G.; Azad, A. K. Proton-conducting electrolytes for direct methanol and direct urea fuel cells—A state-of-the-art review. *Renewable Sustainable Energy Rev.* **2016**, *57*, 1347—1358.
- (8) Nguyen, N. S.; Das, G.; Yoon, H. H. Nickel/cobalt oxide-decorated 3D graphene nanocomposite electrode for enhanced electrochemical detection of urea. *Biosens. Bioelectron.* **2016**, 77, 372–377
- (9) Yu, Z.-Y.; Lang, C.-C.; Gao, M.-R.; Chen, Y.; Fu, Q.-Q.; Duan, Y.; Yu, S.-H. Ni-Mo-O nanorod-derived composite catalysts for efficient alkaline water-to-hydrogen conversion via urea electrolysis. *Energy Environ. Sci.* **2018**, *11*, 1890–1897.
- (10) Yan, W.; Wang, D.; Botte, G. G. Electrochemical decomposition of urea with Ni-based catalysts. *Appl. Catal., B* **2012**, *127*, 221–226.
- (11) Jia, H.; Yao, Y.; Zhao, J.; Gao, Y.; Luo, Z.; Du, P. A novel twodimensional nickel phthalocyanine-based metal—organic framework for highly efficient water oxidation catalysis. *J. Mater. Chem. A* **2018**, *6*, 1188—1195.
- (12) Zhan, S.; Zhou, Z.; Liu, M.; Jiao, Y.; Wang, H. 3D NiO nanowalls grown on Ni foam for highly efficient electro-oxidation of urea. *Catal. Today* **2019**, 327, 398–404.
- (13) Zhu, D.; Guo, C.; Liu, J.; Wang, L.; Du, Y.; Qiao, S.-Z. Two-dimensional metal—organic frameworks with high oxidation states for

I

- efficient electrocatalytic urea oxidation. Chem. Commun. 2017, 53, 10906–10909.
- (14) Ma, G.; Xue, Q.; Zhu, J.; Zhang, X.; Wang, X.; Yao, H.; Zhou, G.; Chen, Y. Ultrafine Rh nanocrystals decorated ultrathin NiO nanosheets for urea electro-oxidation. *Appl. Catal., B* **2020**, 265, No. 118567.
- (15) Wang, Z.; Liu, W.; Hu, Y.; Guan, M.; Xu, L.; Li, H.; Bao, J.; Li, H. Cr-doped CoFe layered double hydroxides: Highly efficient and robust bifunctional electrocatalyst for the oxidation of water and urea. *Appl. Catal.*, B **2020**, 272, No. 118959.
- (16) Sayed, E. T.; Eisa, T.; Mohamed, H. O.; Abdelkareem, M. A.; Allagui, A.; Alawadhi, H.; Chae, K.-J. Direct urea fuel cells: Challenges and opportunities. *J. Power Sources* **2019**, 417, 159–175.
- (17) Simka, W.; Piotrowski, J.; Nawrat, G. Influence of anode material on electrochemical decomposition of urea. *Electrochim. Acta* **2007**, *52*, 5696–5703.
- (18) Baker, D. R.; Lundgren, C. A. Expansion of the urea electrocatalytic oxidation window by adsorbed nickel ions. *J. Appl. Electrochem.* **2019**, 49, 883–893.
- (19) Yue, Z.; Zhu, W.; Li, Y.; Wei, Z.; Hu, N.; Suo, Y.; Wang, J. Surface engineering of a nickel oxide—nickel hybrid nanoarray as a versatile catalyst for both superior water and urea oxidation. *Inorg. Chem.* **2018**, *57*, 4693—4698.
- (20) Yang, W.; Yang, X.; Hou, C.; Li, B.; Gao, H.; Lin, J.; Luo, X. Rapid room-temperature fabrication of ultrathin Ni(OH)₂ nanoflakes with abundant edge sites for efficient urea oxidation. *Appl. Catal., B* **2019**, 259, No. 118020.
- (21) Yang, W.; Yang, X.; Li, B.; Lin, J.; Gao, H.; Hou, C.; Luo, X. Ultrathin nickel hydroxide nanosheets with a porous structure for efficient electrocatalytic urea oxidation. *J. Mater. Chem. A* **2019**, *7*, 26364–26370.
- (22) Yuan, M.; Wang, R.; Sun, Z.; Lin, L.; Yang, H.; Li, H.; Nan, C.; Sun, G.; Ma, S. Morphology-Controlled Synthesis of Ni-MOFs with Highly Enhanced Electrocatalytic Performance for Urea Oxidation. *Inorg. Chem.* **2019**, *58*, 11449–11457.
- (23) Vedharathinam, V.; Botte, G. G. Understanding the electrocatalytic oxidation mechanism of urea on nickel electrodes in alkaline medium. *Electrochim. Acta* **2012**, *81*, 292–300.
- (24) Wang, D.; Yan, W.; Botte, G. G. Exfoliated nickel hydroxide nanosheets for urea electrolysis. *Electrochem. Commun.* **2011**, *13*, 1135–1138.
- (25) Boggs, B. K.; King, R. L.; Botte, G. G. Urea electrolysis: direct hydrogen production from urine. *Chem. Commun.* **2009**, 32, 4859–4861
- (26) Yan, W.; Wang, D.; Botte, G. G. Nickel and cobalt bimetallic hydroxide catalysts for urea electro-oxidation. *Electrochim. Acta* **2012**, *61*, 25–30.
- (27) Yan, W.; Wang, D.; Diaz, L. A.; Botte, G. G. Nickel nanowires as effective catalysts for urea electro-oxidation. *Electrochim. Acta* **2014**, *134*, 266–271.
- (28) Ye, K.; Zhang, D.; Guo, F.; Cheng, K.; Wang, G.; Cao, D. Highly porous nickel@carbon sponge as a novel type of three-dimensional anode with low cost for high catalytic performance of urea electro-oxidation in alkaline medium. *J. Power Sources* **2015**, 283, 408–415.
- (29) Shi, W.; Sun, X. J.; Ding, R.; Ying, D. F.; Huang, Y. F.; Huang, Y. X.; Tan, C. N.; Jia, Z. Y.; Liu, E. H. Trimetallic NiCoMo/graphene multifunctional electrocatalysts with moderate structural/electronic effects for highly efficient alkaline urea oxidation reaction. *Chem. Commun.* 2020, 56, 6503–6506.
- (30) Li, B.; Song, C.; Rong, J.; Zhao, J.; Wang, H.-E.; Yang, P.; Ye, K.; Cheng, K.; Zhu, K.; Yan, J.; Cao, D.; Wang, G. A new catalyst for urea oxidation: NiCo₂S₄ nanowires modified 3D carbon sponge. *J. Energy Chem.* **2020**, *50*, 195–205.
- (31) Cook, B. Introduction to fuel cells and hydrogen technology. Eng. Sci. Educ. J. 2002, 11, 205–216.
- (32) Mekhilef, S.; Saidur, R.; Safari, A. Comparative study of different fuel cell technologies. *Renewable Sustainable Energy Rev.* **2012**, *16*, 981–989.

- (33) Zhu, B.; Liang, Z.; Zou, R. Designing Advanced Catalysts for Energy Conversion Based on Urea Oxidation Reaction. *Small* **2020**, *16*. No. 1906133.
- (34) Ganiyu, S. O.; Martínez-Huitle, C. A.; Rodrigo, M. A. Renewable energies driven electrochemical wastewater/soil decontamination technologies: A critical review of fundamental concepts and applications. *Appl. Catal., B* **2020**, *270*, No. 118857.
- (35) Cao, Y.; Wang, K.; Wang, X.; Gu, Z.; Fan, Q.; Gibbons, W.; Hoefelmeyer, J. D.; Kharel, P. R.; Shrestha, M. Hierarchical porous activated carbon for supercapacitor derived from corn stalk core by potassium hydroxide activation. *Electrochim. Acta* **2016**, *212*, 839–847
- (36) Yang, Y.; Chiang, K.; Burke, N. Porous carbon-supported catalysts for energy and environmental applications: A short review. *Catal. Today* **2011**, *178*, 197–205.
- (37) Tsai, W.; Yang, J.; Lai, C.; Cheng, Y.; Lin, C.; Yeh, C. Characterization and adsorption properties of eggshells and eggshell membrane. *Bioresour. Technol.* **2006**, *97*, 488–493.
- (38) Li, Z.; Zhang, L.; Amirkhiz, B. S.; Tan, X.; Xu, Z.; Wang, H.; Olsen, B. C.; Holt, C. M.; Mitlin, D. Carbonized chicken eggshell membranes with 3D architectures as high-performance electrode materials for supercapacitors. *Adv. Energy Mater.* **2012**, *2*, 431–437.
- (39) Nasrollahzadeh, M.; Sajadi, S. M.; Hatamifard, A. Waste chicken eggshell as a natural valuable resource and environmentally benign support for biosynthesis of catalytically active Cu/eggshell, Fe₃O₄/eggshell and Cu/Fe₃O₄/eggshell nanocomposites. *Appl. Catal., B* **2016**, *191*, 209–227.
- (40) Lu, S.; Hummel, M.; Gu, Z.; Gu, Y.; Cen, Z.; Wei, L.; Zhou, Y.; Zhang, C.; Yang, C. Trash to treasure: A novel chemical route to synthesis of NiO/C for hydrogen production. *Int. J. Hydrogen Energy* **2019**, *44*, 16144–16153.
- (41) Lu, S.; Gu, Z.; Hummel, M.; Zhou, Y.; Wang, K.; Xu, B. B.; Wang, Y.; Li, Y.; Qi, X.; Liu, X. Nickel Oxide Immobilized on the Carbonized Eggshell Membrane for Electrochemical Detection of Urea. J. Electrochem. Soc. 2020, 167, No. 106509.
- (42) Maruthapandian, V.; Kumaraguru, S.; Mohan, S.; Saraswathy, V.; Muralidharan, S. An Insight on the Electrocatalytic Mechanistic Study of Pristine Ni MOF (BTC) in Alkaline Medium for Enhanced OER and UOR. *ChemElectroChem* **2018**, *5*, 2795–2807.
- (43) Ye, K.; Wang, G.; Cao, D.; Wang, G. Recent advances in the electro-oxidation of urea for direct urea fuel cell and urea electrolysis. *Top. Curr. Chem.* **2018**, *376*, No. 42.
- (44) Perdew, J. P.; Burke, K.; Ernzerhof, M. Generalized gradient approximation made simple. *Phys. Rev. Lett.* **1996**, *77*, No. 3865.
- (45) Kresse, G.; Hafner, J. Norm-conserving and ultrasoft pseudopotentials for first-row and transition elements. *J. Phys.: Condens. Matter* **1994**, *6*, 8245–8257.
- (46) Panchal, M.; Raghavendra, G.; Ojha, S.; Omprakash, M.; Acharya, S. A single step process to synthesize ordered porous carbon from coconut shells-eggshells biowaste. *Mater. Res. Express* **2019**, *6*, No. 115613.
- (47) Liu, H.; Wang, G.; Liu, J.; Qiao, S.; Ahn, H. Highly ordered mesoporous NiO anode material for lithium ion batteries with an excellent electrochemical performance. *J. Mater. Chem.* **2011**, *21*, 3046–3052.
- (48) Zhai, Z.; Liu, Q.; Zhu, Y.; Cao, J.; Shi, S. Synthesis of Ni(OH)₂/graphene composite with enhanced electrochemical property by stirring solvothermal method. *J. Alloys Compd.* **2019**, 775, 1316–1323.
- (49) Aghazadeh, M.; Golikand, A. N.; Ghaemi, M. Synthesis, characterization, and electrochemical properties of ultrafine β -Ni(OH)₂ nanoparticles. *Int. J. Hydrogen Energy* **2011**, *36*, 8674–8679
- (50) Su, Y.-Z.; Xiao, K.; Li, N.; Liu, Z.-Q.; Qiao, S.-Z. Amorphous Ni (OH)2@three-dimensional Ni core—shell nanostructures for high capacitance pseudocapacitors and asymmetric supercapacitors. *J. Mater. Chem. A* **2014**, *2*, 13845–13853.
- (51) Tong, Y.; Chen, P.; Zhang, M.; Zhou, T.; Zhang, L.; Chu, W.; Wu, C.; Xie, Y. Oxygen vacancies confined in nickel molybdenum

oxide porous nanosheets for promoted electrocatalytic urea oxidation. ACS Catal. 2018, 8, 1–7.

- (52) Daramola, D. A.; Singh, D.; Botte, G. G. Dissociation rates of urea in the presence of NiOOH catalyst: a DFT analysis. *J. Phys. Chem. A* **2010**, *114*, 11513–11521.
- (53) Zhu, X.; Dou, X.; Dai, J.; An, X.; Guo, Y.; Zhang, L.; Tao, S.; Zhao, J.; Chu, W.; Zeng, X. C.; Xie, Y.; Wu, C. Metallic nickel hydroxide nanosheets give superior electrocatalytic oxidation of urea for fuel cells. *Angew. Chem., Int. Ed.* **2016**, *55*, 12465–12469.